*** 研究論文 ***

コンピュータオブザーバを用いた Anatomical-MAP 画像再構成法の病変検出能評価

小林 哲哉[*1] 工藤 博幸[*1]

要 旨

本研究では，放射型 CT における形態情報を利用した Anatomical-MAP 画像再構成法の病変検出能を，コンピュータオブザーバと呼ばれる数値計算による観測者モデルを用いて評価する．病変検出のタスクに対する従来の Anatomical-MAP 法の問題点は，形態情報として利用する CT／MR 画像に写っていない病変のコントラストを保存したまま，滑らかな濃度変化をもつ背景の雑音を抑制する効果がないことである．これに対して，筆者らは放射能分布画像を滑らかな背景画像と疎なスポット画像の和として表現する Spots-on-smooth モデルに基づく Anatomical-MAP 再構成法（SOS-MAP）を提案し［8, 9］，病変のコントラストを保存したまま背景の雑音を抑制することを可能にした．本論文では，これまで明らかでなかった SOS-MAP 法の病変検出能をコンピュータオブザーバによって評価し，従来手法と比較して優れた病変検出能をもつことを示す．

キーワード：放射型 CT，画像再構成，形態情報，病変検出，コンピュータオブザーバ
Med Imag Tech **28** (4) : 214-222, 2010

1. はじめに

PET や SPECT などの放射型 CT（Emission CT, ECT）では最尤推定（Maximum Likelihood, ML）に基づく統計的画像再構成法［1, 2］の導入により画質が改善した．しかし，ここでの画質改善とはフィルタ補正逆投影法などの解析的手法と比較した場合の相対的なものであり，空間分解能や信号対雑音比などの絶対的な画像性能は依然として低い．そこで，さらなる画質改善を目的に，ML の自然な拡張として最大事後確率推定（Maximum A *Posteriori*; MAP）に基づく画像再構成［2 - 4］が古くから研究されてきた．MAP 再構成とは，対象画像が普遍的にもつ性質（先験情報）を事前確率として定式化し，ベイズの定理から得られる事後確率の最大化解として画像を得る手法である．既存の MAP 再構成法の多くは，統計雑音を抑制するために，対象画像の局所的な濃度変化が小さいことを先験情報として利用している．ただし，この手法には濃度変化の大きなエッジを保存できない欠点がある．この欠点を補うため Anatomical-MAP（A-MAP）再構成［5, 6］と呼ばれる手法が提案された．A-MAP 法は ECT 画像に現れる機能的な境界と生体内の解剖学的境界がほぼ一致すると仮定し，同一対象の高分解能な形態画像（CT/ MR）がもつ境界情報を事前確率に反映させてエッジ保存性を高める手法である．しかし，腫瘍などの機能的な異常は形態画像に写らない場合が多く，病変検出を目的とした撮影において従来の A-MAP 法を利用する効果は非常に小さいとされている［7］．

これに対して，筆者らは腫瘍などのスポット状の異常集積の検出に特化した巧妙な MAP 再構成法を提案した［8, 9］．本手法では放射能分布画像 $\mathbf{x}$ を，正常部位を表す背景画像 $\mathbf{b}$ と病変を表すスポット画像 $\mathbf{s}$ の和 $\mathbf{b}+\mathbf{s}$ として表現する Spots-on-smooth（SOS）モデル［10］に基づき（**Fig. 1**），背景画像とスポット画像を独立な画像として分離して再構成する．本論文ではこの手法を SOS-MAP 法と呼ぶ．SOS-MAP 法の特徴は，背景画像は滑らかで，スポット画像は疎（スパース）である（ほとんどの画素値がゼロである）という仮定を設け，その先験情報を MAP 再構成に組み込むことで正常画像と病変画像を高精度に推定しようとする点にある．また，SOS-MAP 法

[*1] 筑波大学大学院システム情報工学研究科コンピュータサイエンス専攻〔〒 305-8573 つくば市天王台 1-1-1〕
e-mail: kobayashi@imagelab.cs.tsukuba.ac.jp
投稿受付：2010 年 5 月 14 日
最終稿受付：2010 年 8 月 24 日
採用決定日：2010 年 8 月 25 日

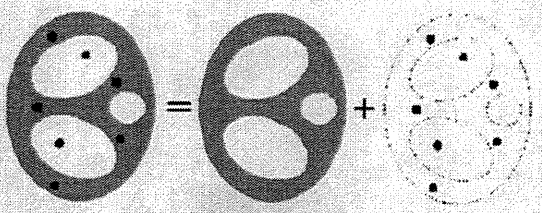

Fig. 1 Spots-on-smooth image model[10].

は病変部位を含まない背景画像の推定に形態情報を利用するため，従来の A-MAP 法と異なり，形態画像に写っていない病変をもつ画像に対しても画質改善効果がある．さらに，SOS-MAP 法は病変候補となるスポット状の異常集積を周囲の正常領域から分離して再構成するため，画像再構成と病変検出を統合する ECT の新しいイメージング概念を示すものである．

筆者らは，先行研究 [9] において SOS-MAP 法の物理的な画像性能（コントラスト対雑音特性）を評価し，従来の A-MAP 法に対する優位性を示した．一方で，人間の主観的な判断による病変の検出しやすさ，すなわち病変検出能という観点での画質評価も重要である．そこで，本研究では，コンピュータオブザーバと呼ばれる数値計算による観測者モデルを用いて SOS-MAP 法の病変検出能を評価し，従来の A-MAP 法と性能を比較する．

本論文の構成は以下に示すとおりである．2. では，4. で述べる病変検出能評価実験の準備として，SOS-MAP 法と従来の A-MAP 法について説明する．3. ではコンピュータオブザーバについて説明する．4. ではコンピュータオブザーバを用いた病変検出能評価実験の方法および結果を示す．5. では考察を述べ，6. でまとめとする．

2. Anatomical-MAP 再構成

1) SOS-MAP 法 [8, 9]

まず，SOS-MAP 法による画像再構成を定式化する．対象画像を $\mathbf{x} \in \mathrm{R}^N$，背景画像を $\mathbf{b} \in \mathrm{R}^N$，スポット画像を $\mathbf{s} \in \mathrm{R}^N$ で表し，$\mathbf{x} = \mathbf{b} + \mathbf{s}$ とする．また，投影データを $\mathbf{y} \in \mathrm{R}^M$，投影演算を $M \times N$ 行列 $A=\{a_{ij}\}$ で表す．SOS-MAP 法では，以下の最小化問題として画像再構成を定式化する．

$$\begin{aligned} &\text{minimize } F(\mathbf{b},\mathbf{s}) \\ &\text{subject to } \mathbf{b} \geq 0, \mathbf{b}+\mathbf{s} \geq 0 \\ &F(\mathbf{b},\mathbf{s}) = L(\mathbf{b},\mathbf{s}) + \beta_1 U_1(\mathbf{b}) + \beta_2 U_2(\mathbf{s}) + \gamma D(\mathbf{s}) \end{aligned} \tag{1}$$

ここで，$L(\mathbf{b},\mathbf{s})$ は測定データの対数尤度，$U_1(\mathbf{b})$, $U_2(\mathbf{s})$ はおのおの背景画像とスポット画像の平滑化関数，$D(\mathbf{s})$ はスポット画像のスパース性を評価する関数である．β_1, β_2, γ は対応するペナルティ関数の重みパラメータである．対数尤度および 3 つのペナルティ関数は，以下のように定義される．

$$\begin{aligned} L(\mathbf{b},\mathbf{s}) &= \sum_{i=1}^{M} [\underline{y}_i(\mathbf{b}+\mathbf{s}) - y_i \log \underline{y}_i(\mathbf{b}+\mathbf{s})] \\ U_1(\mathbf{b}) &= \sum_{j=1}^{N} (b_j - m_j(\mathbf{b}))^2 / 2 \\ U_2(\mathbf{s}) &= \sum_{j=1}^{N} \sum_{l \in S_j} \varphi(s_j - s_l)/d_{jl} \\ D(\mathbf{s}) &= \sum_{j=1}^{N} l_0(s_j) \end{aligned} \tag{2}$$

ただし，S_j はスポット画像の画素 j の近傍画素集合，d_{jl} は画素 j と画素 l のユークリッド距離である．本研究では，クリークポテンシャル $\varphi(r)$ として，一般的な 2 次ポテンシャル $\varphi(r) = r^2/2$ を用いる．また，式 (2) において $\underline{y}_i(\cdot)$, $m_j(\mathbf{b})$, $l_0(s_j)$ は以下のように定義される．

$$\begin{aligned} \underline{y}_i(\mathbf{x}) &= \sum_{j=1}^{N} a_{ij} x_j \\ m_j(\mathbf{b}) &= \arg\min_{m} \sum_{k \in B_j} w_{jl} |m - b_l| \\ l_0(s_j) &= \lim_{p \to +0} |s_j|^p \quad \text{(L0 norm)} \end{aligned} \tag{3}$$

ここで，$m_j(\mathbf{b})$ は背景画像の画素 j の近傍画素集合 B_j に属する画素値の加重中央値である．w_{jl} は画素対 (j,l) の相関を表す係数であり，今回は CT 画像 $\mu \in \mathrm{R}^N$ を利用して次式により定義する．

$$w_{jl} = \frac{\exp[-(\mu_j - \mu_l)^2/\sigma^2]}{\sum_{k \in B_j} \exp[-(\mu_j - \mu_k)^2/\sigma^2]} \tag{4}$$

ただし，$\sigma > 0$ は CT 画像中のエッジを背景画像にどの程度シャープに再現するかを調節するパラメータである．

次に，式 (1) の最小化問題を解く逐次近似法について説明する．評価関数 $F(\mathbf{b},\mathbf{s})$ は背景画像 $\mathbf{b}$ とスポット画像 $\mathbf{s}$ を変数にもつが，両者を同時に最適化することは困難である．そこで，SOS-MAP 法では交互最小化法を用いる．具体的には，$\mathbf{s}$ を現在の近似解に固定して $\mathbf{b}$ を更新する [Step 1]，$\mathbf{b}$ を現在の近似解に固定して $\mathbf{s}$ を更新する [Step 2]，という 2 ステップからなる計算を交互に繰り返す構造をもつ (Fig. 2)．背景画像とスポット画

像の更新ステップ [Step 1], [Step 2] において最小化する関数は，以下のように簡単になる．

$$\begin{aligned}&\text{[Step 1]}\ F_b(\mathbf{b};\underline{\mathbf{s}}) = L(\mathbf{b},\underline{\mathbf{s}}) + \beta_1 U_1(\mathbf{b})\\ &\text{[Step 2]}\ F_s(\mathbf{s};\underline{\mathbf{b}}) = L(\underline{\mathbf{b}},\mathbf{s}) + \beta_2 U_2(\mathbf{s}) + \gamma D(\mathbf{s})\end{aligned} \tag{5}$$

ただし，$\underline{\mathbf{b}}$, $\underline{\mathbf{s}}$ は $\mathbf{b}$, $\mathbf{s}$ の現在の近似解を表す．$F_b(\mathbf{b};\underline{\mathbf{s}})$ の最小化は式 (6)，$F_s(\mathbf{s};\underline{\mathbf{b}})$ の最小化は式 (7) の反復計算により行う．

$$\begin{aligned}&\hat{b}_j^{(k,p)} = b_j^{(k,p)} - \frac{\left(\frac{\partial L}{\partial b_j} + \beta_1 \frac{\partial U_1}{\partial b_j}\right)\Big|_{\mathbf{b}=\mathbf{b}^{(k,p)},\,\mathbf{s}=\underline{\mathbf{s}}}}{\sum_{i=1}^{M} a_{ij} \Big/ \left(b_j^{(k,p)} + \underline{s}_j\right) + 2\beta_1}\\ &b_j^{(k,p+1)} = \max\left(\hat{b}_j^{(k,p)}, \max(0, -\underline{s}_j)\right)\end{aligned} \tag{6}$$

$$\begin{aligned}&\hat{s}_j^{(k,q)} = s_j^{(k,q)} - \frac{\left(\frac{\partial L}{\partial s_j} + \beta_2 \frac{\partial U_2}{\partial s_j}\right)\Big|_{\mathbf{s}=\mathbf{s}^{(k,q)},\,\mathbf{b}=\underline{\mathbf{b}}}}{\sum_{i=1}^{M} a_{ij} \Big/ \left(\underline{b}_j + s_j^{(k,q)}\right)}\\ &t_j = \sum_{i=1}^{M} a_{ij} \Big/ \left[2\gamma\left(\underline{b}_j + s_j^{(k,q)}\right)\right]\\ &s_j^{(k,q+1)} = \begin{cases} \max(\hat{s}_j^{(k,q)}, -\underline{b}_j) & (|\hat{s}_j^{(k,q)}| < \sqrt{1/t_j}) \\ 0 & (|\hat{s}_j^{(k,q)}| \geq \sqrt{1/t_j}) \end{cases}\end{aligned} \tag{7}$$

ただし，p, q はおのおの [Step 1] と [Step 2] の内部反復回数，k は全体の反復回数である．式 (6),(7) の説明や導出は文献 [9, 10, 15] を参照されたい．

SOS-MAP 法では，背景画像の近傍画素集合 B_j を，検出するスポット状の異常集積の大きさよりも十分大きく設定し，平滑化関数 $U_1(\mathbf{b})$ の重み β_1 を大きな値に設定することにより，異常集積を意図的に背景画像から除去し，滑らかな濃度変化をもつ背景画像を推定する．一方，背景画像から除去された異常集積は正常領域の値から大きく外れた値であり，スポット画像の L0 ノルム $D(\mathbf{s})$ を評価関数に加えたことから生じる式 (7) の閾値処理（外れ値検出）によりスポット画像上に高いコントラストで復元する．これらのことから，SOS- MAP 法では，3 つの正則化パラメータ β_1, β_2, γ の設定が重要である．β_1 は背景画像の平滑化の強さを決めるパラメータ，β_2 はスポット画像の平滑化の強さを決めるパラメータ，γ はスポット画像に病変を検出する際の閾値パラメータである．4. でこれらの正則化パラメータの画質への影響を考察する．

2）従来の A-MAP 法

従来の A-MAP 法では，以下の最小化問題として画像再構成を定式化する．

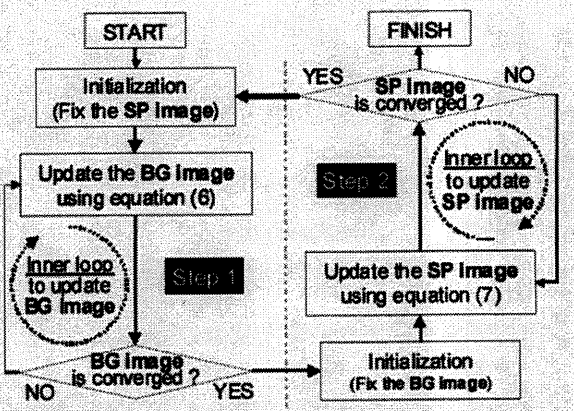

Fig. 2 The flowchart of the SOS-MAP reconstruction method. The abbreviations BG and SP represent background and spot, respectively.

$$\begin{aligned}&\text{minimize}\ F(\mathbf{x}) = L(\mathbf{x}) + \beta U(\mathbf{x})\\ &\text{subject to}\ \mathbf{x} \geq 0\\ &L(\mathbf{x}) = \sum_{i=1}^{M}\left[\underline{y}_i(\mathbf{x}) - y_i \log \underline{y}_i(\mathbf{x})\right]\\ &U(\mathbf{x}) = \sum_{j=1}^{N}\sum_{l\in N_j} w_{jl}\varphi(x_j - x_l)\end{aligned} \tag{8}$$

ただし，$L(\mathbf{x})$ は測定データの対数尤度，$U(\mathbf{x})$ は平滑化関数，β は $U(\mathbf{x})$ の重みを調節するパラメータである．N_j は画素 j の近傍画素集合，w_{jl} は画素対 (j,l) の相関を表す係数であり，今回は式 (4) の w_{jl} と同一とする．本研究では，具体的なポテンシャル関数 $\varphi(r)$ の形として 2 次ポテンシャルと次式のエッジ保存型ポテンシャルを用いる．

$$\varphi(r) = \delta^2\left[|r/\delta| - \log(1+|r/\delta|)\right] \tag{9}$$

ただし，$\delta > 0$ は定性的には隣接画素間の平滑化を行うか行わないかを決定する閾値である．$F(\mathbf{x})$ の最小化は，以下の反復計算により行う．

$$x_j^{(k+1)} = \left[x_j^{(k)} - \frac{\left(\frac{\partial L}{\partial x_j} + \beta\frac{\partial U}{\partial x_j}\right)\Big|_{\mathbf{x}=\mathbf{x}^{(k)}}}{\sum_{i=1}^{M} a_{ij} \Big/ x_j^{(k)} + 2\beta}\right]^{+} \tag{10}$$

ただし，$[\cdot]^+$ は負の値をゼロに置換する演算，k は反復回数を表す．式 (10) において $\beta = 0$ とすると MLEM 法 [1] の反復式が得られる．式 (10) の導出は文献 [15] を参照されたい．

3. コンピュータオブザーバ

病変検出能評価は人間による主観評価実験に基づいて行うことが理想的であるが，さまざまな撮影条件下で主観評価実験を繰り返し行うことは困難な場合が多い．そこで，人間による識

別をモデル化し，数値計算により病変検出能を評価するコンピュータオブザーバ (Computer Observer; COB) という考え方が提案された[12]. COB を用いた病変検出能評価は，一般に病変あり画像群と病変なし画像群の 2 群を仮定する. COB の病変検出能とは，2 つの画像群の空間的な重なりの小ささを 2 群の分離能として数値化したものである.

1) Channelized Hotelling Observer

本論文では，SKE-BKE(Signal known exactly, Background known exactly) という仮定のもとで病変検出能を評価する CHO (Channelized Hotelling Observer) [13] と呼ばれる COB を用いる. まず，SKE-BKE モデルとは，信号の背景成分（病変なし画像）の統計的性質（平均や共分散）が既知であり，さらに信号（病変）の位置も既知であると仮定するモデルである. これは雑音が多い画像を見て，所定の位置に病変が有るか無いかを判断するタスクを想定している. 実際の病変検出では信号位置を特定するタスクも同時に行う必要があるが，その場合，評価実験や病変検出能の数学的取扱いが複雑になるため，COB を用いた評価実験の多くが SKE-BKE モデルを採用している. CHO はデータ群の平均と共分散を情報に信号の有無を判断する Hotelling observer の一種である. Channelized とは，画像信号にバンドパスフィルタ（BP フィルタ）を通して得られる帯域信号を直接の観測データとすることを意味している. CHO がもつフィルタリング機構は，人間の視覚システムが周波数応答特性の異なる複数のチャンネルによって物体を認識するという仮説に由来する. CHO の病変検出能指標 d_{CHO} の計算手順を以下に示す.

(a) 同一の測定および再構成条件において生成された病変あり画像と病変なし画像をおのおの P 枚準備する.

(b) 各画像群のすべての画像を N_c 種類の BP フィルタに通して N_c 次元の帯域信号に変換する. 病変あり画像，なし画像の帯域信号をおのおの $\mathbf{f}_p^i, \mathbf{f}_a^i\ (i=1,2,\cdots,P)$ とおく.

(c) 各データ群の平均ベクトル $\mathbf{f}_p, \mathbf{f}_a$ と共分散行列 Σ_p, Σ_a を求める.

(d) 各データ群の全標本に対して，次式で定義される検定統計量 $\lambda_p(i), \lambda_a(i)\ (i=1,2,\cdots,P)$ を計算する. 検定統計量は信号に対する観測者の応答を数値化したものである.

$$\lambda_h(i)=(\mathbf{f}_p-\mathbf{f}_a)\Sigma^{-1}\mathbf{f}_h^i \quad (h=p,a) \tag{11}$$

ここで，行列 Σ は各データ群の共分散行列 Σ_p, Σ_a を平均した行列を表す.

(e) 各群の検定統計量の平均 $\bar{\lambda}_p, \bar{\lambda}_a$ および分散 σ_p^2, σ_a^2 を計算し，次式で定義される病変検出能指標 d_{CHO} を算出する.

$$d_{CHO}=\left|\bar{\lambda}_p-\bar{\lambda}_a\right|\Big/\sqrt{\tfrac{1}{2}(\sigma_p^2+\sigma_a^2)} \tag{12}$$

2) 周波数応答モデル

周波数応答特性をもつ COB では，Square, Difference-of-Gaussian, Laguerre-Gauss などの周波数応答モデルが用いられる. 本研究では，もっとも一般的な Square (SQR) モデル [13] を用いる. SQR モデルに対応する BP フィルタ $h_c(x,y)\ (c=1,2,\cdots,N_c)$ は周波数空間において次式で定義される.

$$H_c(u,v)=\begin{cases}1 & (\rho_0 2^{c-1}\le\sqrt{u^2+v^2}\le\rho_0 2^c)\\ 0 & (\text{otherwise})\end{cases} \tag{13}$$

ただし，ρ_0 [pixel^{-1}] はカットオフ周波数である. $H_c(u,v)$ をフーリエ逆変換すると，実空間の BP フィルタ $h_c(x,y)$ が以下のように求められる.

$$h_c(x,y)=\begin{cases}\left[bJ_1(2\pi br)-aJ_1(2\pi ar)\right]/r & (r\neq 0)\\ \pi(b^2-a^2) & (r=0)\end{cases} \tag{14}$$
$$\left(r=\sqrt{x^2+y^2}, a=\rho_0 2^{c-1}, b=\rho_0 2^c\right)$$

ただし，$J_1(x)$ は第 1 種ベッセル関数である. 本論文の評価実験で使用した SQR モデルの BP フィルタを **Fig. 3** に示す.

4. 病変検出能評価実験

本研究における病変検出能評価実験の目的は，(1) SOS-MAP 法がもつ正則化パラメータ β_1, β_2, γ の値と病変検出能の関係を調べること，(2) SOS-MAP 法と従来の A-MAP 法の病変検出能の比較，の 2 つである.

1) 実験方法

2 次元 PET の画像再構成を想定して，病変検出能評価に用いる 2 つの画像群データを生成した. 投影データの生成に用いた数値ファントム [11] およびエッジ情報として再構成に用いた CT 画像を **Fig. 4** に示す. ファントム画像のサイズは 384×384 (1.35 [mm/pixel]) であり，FDG-PET 検査における胸部の放射能分布を模擬している. 検

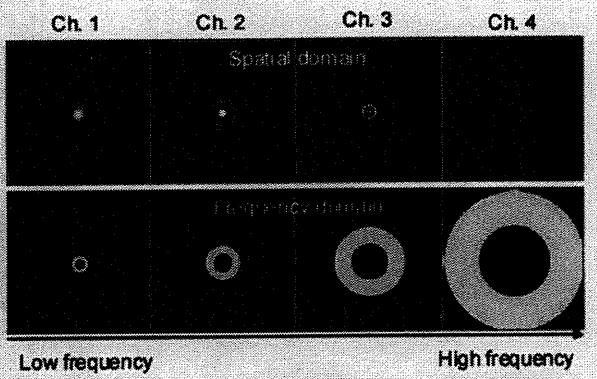

Fig. 3 Spatial and frequency response functions of the square channel model used in this paper (ρ_0=0.03125, N_c = 4).

出対象とする病変は直径 13.5[mm] の 2 つの腫瘍 (Tumor 1, Tumor 2) である．ファントムは同一領域内で滑らかな濃度変化をもち，肺，肺を囲む体幹部，腫瘍の放射能濃度比は約 1:2:3 とした．投影データのサイズは 128×128 (検出器のビン幅 4.05[mm]) である．投影データは物体による γ 線光子の吸収を考慮した上で，検出器特性はガウシアン応答モデル (半値幅 6.075[mm]) を用いて計算し，全計数値 1M カウントに相当するポアソン雑音を加えた．吸収補正は投影データ計算時に仮定した γ 線吸収を画像再構成の際にシステム行列 A に含めることで行った．再構成画像のサイズは 128×128 (4.05 [mm/pixel]) とし，画像再構成の反復計算終了後に半値幅 6.075[mm] (1.5 画素) のガウシアンフィルタによる平滑化を行った．

SOS-MAP 法と従来の A-MAP 法のすべての再構成パラメータの値を **Table 1** に示す．SOS-MAP 法では β_1, β_2, γ の値をおのおの 4 つ準備し，すべての組み合わせ (64 通り) で再構成を行った．SOS-MAP 法と従来の A-MAP 法において CT 画像のエッジ再現性を調節するパラメータ σ の値が異なるが，それらの値は予備的な実験に基づき決定した．また，形態情報を利用しない場合として，ECT の標準的な再構成法である Post-smoothed ML-EM (100 反復，サブセット数 4) による再構成も行った．病変あり画像と病変なし画像はおのおの 100 枚準備した (P=100)．CHO のチャンネル数は N_c = 4，カットオフ周波数は ρ_0 = 0.03125 [pixel^{-1}] とした．これらの値は文献 [14] で用いられた値である．本実験では，2 つの腫瘍の検出能を個別に評価するため，おのおのの腫瘍を中心とした 63×63 の領域を CHO の入力画像とした．

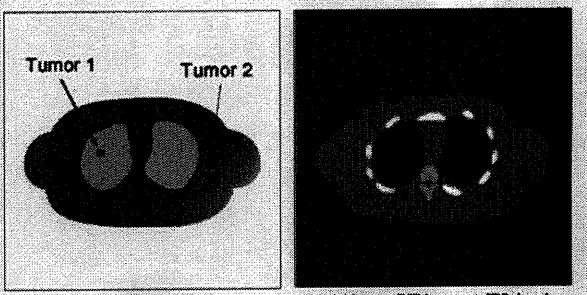

(a) Emission image (384 × 384)　(b) X-ray CT image (70 kev) (128 × 128)

Fig. 4 (a) The emission image used in the simulation study. (b) The X-ray CT image used as edge information in the reconstruction.

Table 1 Parameter settings of the SOS-MAP method and the conventional A-MAP methods with two different potential functions.

SOS-MAP	
β_1	4, 8, 16, 32
β_2 ×0.01	4, 8, 16, 32
γ ×0.001	4, 8, 12, 16
B_j	Circular region of 7 pixels in diameter
S_j	3×3
σ	0.02 [mm^{-1}]
# of local iterations in Step 1	Terminated when $\|\mathbf{b}^{(k,p+1)} - \mathbf{b}^{(k,p)}\|_1 / \|\mathbf{b}^{(k,p)}\|_1 < 0.006$ is satisfied.
# of local iterations in Step 2	100
# of global iterations	5

A-MAP with the quadratic potential	
β ×0.01	2^p (p=2,3,...,12)
N_j	3×3
σ	0.04 [mm^{-1}]
# of iterations	100 (4 subsets)

A-MAP with the edge-preserving potential	
β ×0.01	2^p (p=6,7,...,13), $2^{11.5}$, $2^{12.5}$
δ	0.01
N_j	3×3
σ	0.04 [mm^{-1}]
# of iterations	100 (4 subsets)

2) 実験結果

まず，各再構成法によって得られた病変あり

画像の1例を **Fig. 5** に示す．表示グレースケールはすべての画像で同一にしてある．次に，SOS-MAP 法による Tumor 1 の病変検出能を γ の値に対してプロットしたグラフを **Fig. 6** に示す．Tumor 2 の病変検出能も **Fig. 6** と同様な傾向を示したので，ここでは割愛する．最後に，腫瘍のコントラストに相当する Tumor-to-Background (T/B) 比に対して病変検出能をプロットしたグラフを **Fig. 7** に示す．ただし，T/B 比は次式で定義される．

$$\text{T/B ratio} = \frac{\left\langle x_j^p(i) \right\rangle_{i\in[1,P],j\in R_s}}{\left\langle x_j^a(i) \right\rangle_{i\in[1,P],j\in R_s}} \tag{15}$$

ここで，$x_j^p(i), x_j^a(i)$ はおのおの病変あり画像と病変なし画像の画素値を表し，j は画素番号，i は各画像群に属するサンプルの番号を表す．R_s は腫瘍を中心とした 3×3 [pixels] の領域である．**Fig. 7** では1つの β_1 の値をもつ SOS-MAP 法に対して同じ線種のグラフが 4 本存在するが，おのおの β_2 の値が異なる場合を表している．具体的には，図中の矢印の方向（T/B 比が減る方向）に β_2 の値が増加する．また，観測データの統計雑音が大きい場合として，全計数値が 0.5M の場合の結果を **Fig. 7(b)** に示す．1M の場合は全計数値に対して約 10%, 0.5M の場合は約 15% の統計雑音が含まれており，両設定ともに臨床条件に則した設定となっている．

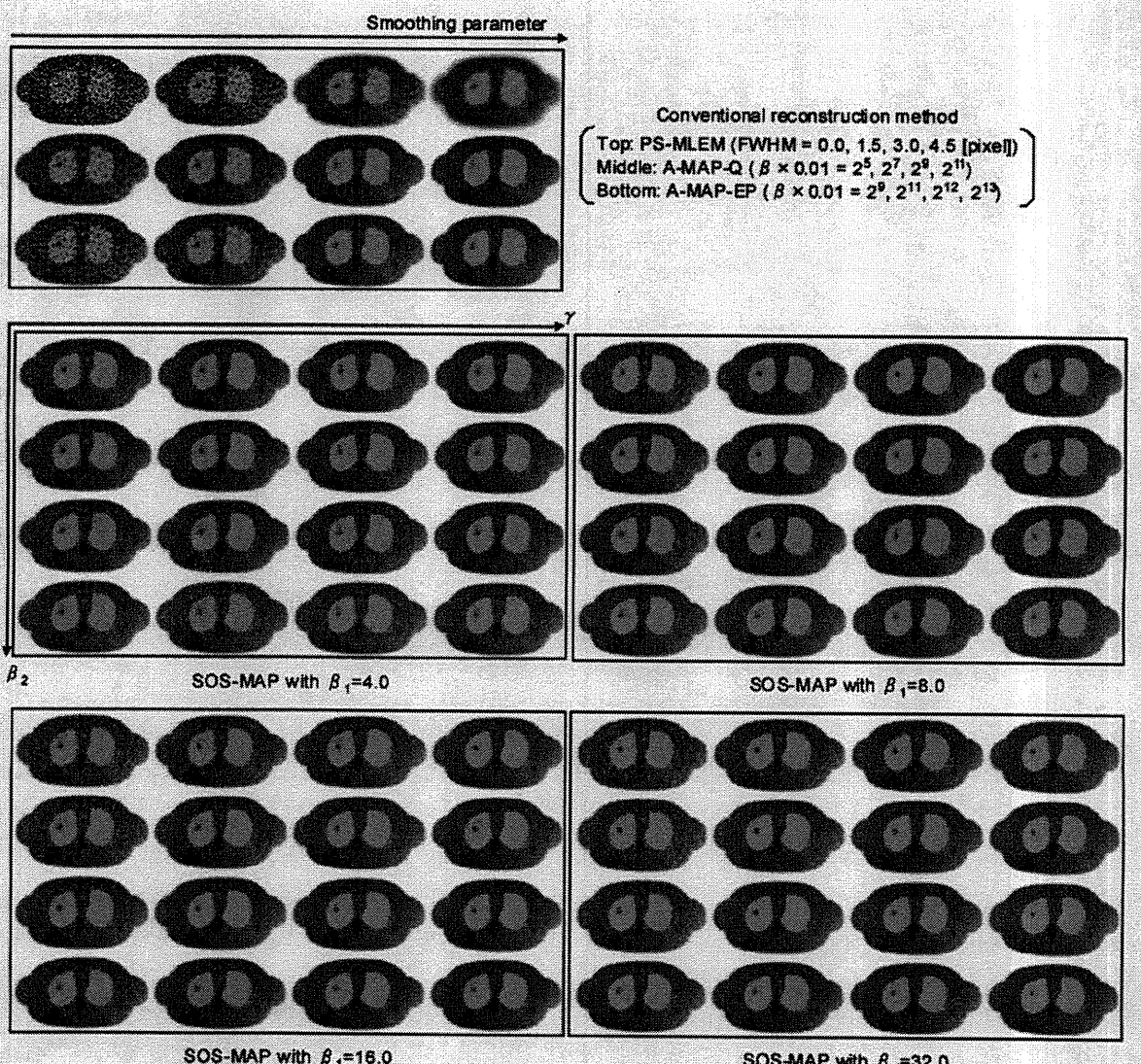

Fig. 5 The reconstructed images of the 1M counts data by the SOS-MAP method and the conventional reconstruction methods with different reconstruction/smoothing parameters. PS-MLEM, A-MAP-Q and A-MAP-EP are short for the post-smoothed MLEM, the A-MAP methods with the quadratic and edge-preserving potential functions, respectively.

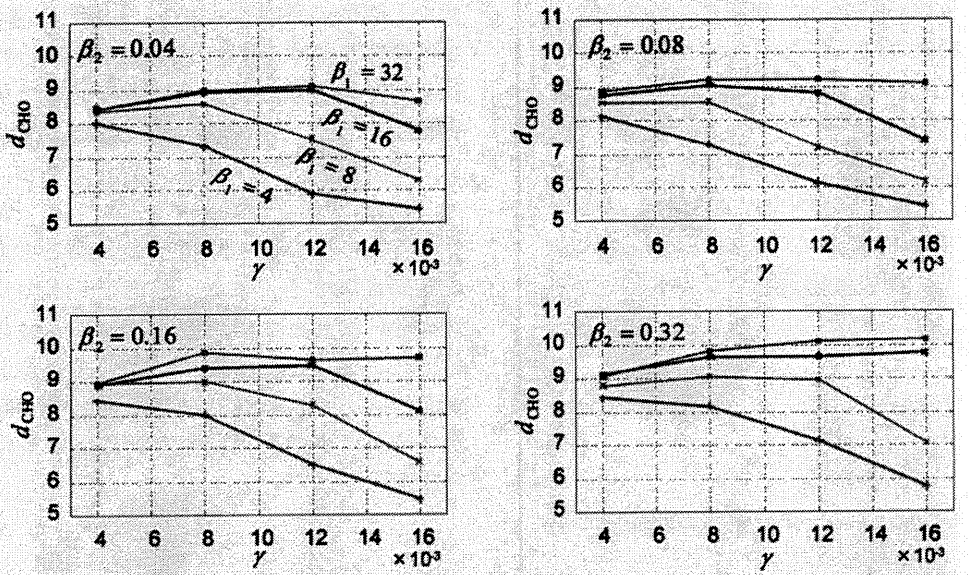

Fig. 6 CHO detectability of the SOS-MAP method with different hyper-parameters (β_1, β_2, γ). The detectability of the tumor 1 in the reconstruction of 1M counts data is shown here.

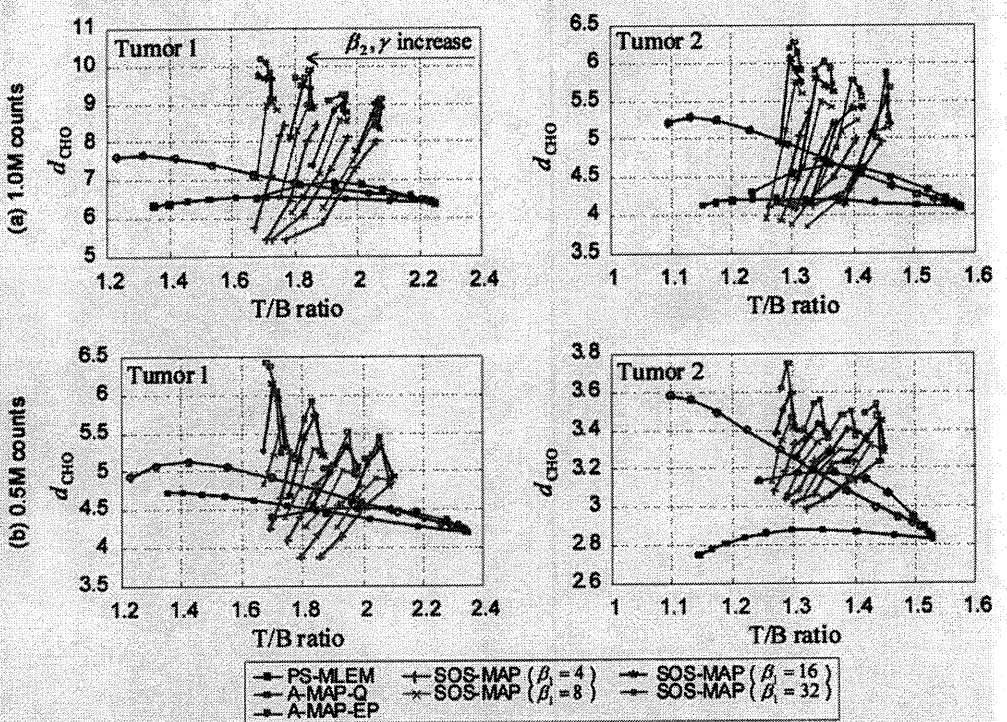

Fig. 7 Plots of CHO detectability versus T/B ratio of all the reconstruction methods in this study.

5. 考 察

まず，SOS-MAP 法の病変検出能について考察する．**Fig. 6** より，SOS-MAP 法の病変検出能は背景画像の滑らかさを決める β_1 の値とスポット検出の閾値を決める γ の値の組み合わせに大きく依存することがわかる．β_1 の値が小さい場合，γ の値が大きくなるにしたがって病変検出能は単調に低下する．これは以下の理由のためである．SOS-MAP 法では β_1 の値が小さすぎると背景画像からスポット領域を十分に除去することができず，背景画像上に中途半端に残ってしまう．その結果，スポット画像の推定は定性的には対象画像 **x** と背景画像 **b** の差分計算であるから，背景画像の精度低下がスポット画像の精度低下を

引き起こす．実際に，**Fig. 5** において β_1=4 と β_1=32 の再構成画像を比較すると，β_1=4 の画像では γ の値が大きくなるにしたがって，腫瘍部位の大きさが小さくなり識別しにくくなっている．この傾向は β_2 の値が小さいときにより顕著にみられる．一方，β_1=32 の画像では，γ の値が大きくなっても腫瘍の大きさやコントラストは比較的保たれており，さらに正常領域が非常に滑らかであるため，腫瘍部位を識別しやすくなってる．**Fig. 6** の 4 つのグラフは上述の傾向を反映している．

次に，SOS-MAP 法と従来の A-MAP 法の病変検出能を比較する．まず，**Fig. 7** において，従来の A-MAP 法では平滑化パラメータである β の値（PS-MLEM 法ではガウシアンフィルタの半値幅）が大きくなると腫瘍のコントラスト（T/B 比）は低下するが，その代わりに統計雑音が抑制され，病変検出能自体は改善されている．ただし，β や半値幅の値がある程度大きくなると腫瘍のコントラスト低下の影響が病変検出に対して支配的になり，病変検出能は低下に転じる．この平滑化パラメータとコントラスト／病変検出能のトレードオフ関係はSOS-MAP法においても同様に観測され，スポット画像の平滑化パラメータである β_2 の値を大きくすると，腫瘍のコントラストが低下して病変検出能は向上するという現象が起きている（**Fig. 7** を参照）．以上の傾向を踏まえて，SOS-MAP 法と従来の A-MAP 法の病変検出能を考察する．まず，SOS-MAP 法と従来の A-MAP 法の病変検出能の優劣はおのおのの再構成パラメータの値によって逆転する．**Fig. 6** が示すように SOS-MAP 法の病変検出能は β_1 の値が大きい場合に安定するので，β_1=16, 32 の SOS-MAP 法を従来手法との比較対象と考える．このとき，**Fig. 7** が示すように SOS-MAP 法は今回検証したパラメータ β_1, β_2, γ の組み合わせの多くにおいて，従来の A-MAP 法や PS-MLEM 法よりも高い病変検出能を実現している．また，T/B 比と病変検出能の両立という観点においても，SOS-MAP 法の性能は従来手法よりも優れていることがわかる．ただし，β_1=16 の場合は β_2 の値が小さくかつ γ の値が大きいと，つまりスポット画像の平滑化が弱く，スポット検出の閾値が大きいと，病変検出能が低下し従来手法の性能を下回ることがある．この現象は Tumor 2 において顕著であるが，これは Tumor 2 のコントラスト（T/B 比）が Tumor 1 よりも低く，検出が本質的に難しいことに起因する．また，**Fig. 7(a)** と **(b)** の比較から，全計数値が減少すると，SOS-MAP 法と従来手法の病変検出能の差が小さくなることがわかる．これは，SOS-MAP 法が従来手法よりも統計雑音の影響を受けやすいためであり，実際に，全計数値を半減させたことによる検出能の低下率は腫瘍のコントラストや正則化パラメータの設定により若干異なっているが，それらを平均すると従来手法では約 30%，SOS-MAP 法では約 40% であった．

今回の実験結果をまとめると，本実験の測定条件において，SOS-MAP 法の病変検出能は，β_1>16, 0.008<γ< 0.016 というパラメータ値の範囲であれば β_2 の値にかかわらず安定しており，T/B 比や病変の見やすさの視覚評価とのバランスも保たれている．

6. まとめ

本研究では，ECT における Anatomical-MAP 再構成法の病変検出能をコンピュータオブザーバによって評価し，筆者らが提案した SOS-MAP 法が従来の A-MAP 法と比較して優れた病変検出能をもつことを示した．また，SOS-MAP 法の再構成パラメータ β_1, β_2, γ と病変検出能の関係を実験データに基づいて考察し，それらのパラメータの組み合わせが重要であることを示した．この結果は，SOS-MAP 法をうまく動作させるためのパラメータ設定の指標となり，有用な知見であると考えられる．具体的には，以下の 2 つのことが明らかになった．(1) SOS-MAP 法をうまく動作させるには，背景画像の平滑化パラメータ β_1 をスポットが背景に残らないようにある程度大きな値に設定し，スポット画像の閾値パラメータ γ をスポットの誤検出や誤消失が極端に発生しない範囲に設定することが重要である．(2) (1) のように適切にパラメータ設定した SOS-MAP 法の病変検出能は従来の A-MAP 法と比較して優れており，形態画像に写っていない病変についても検出能を改善できる．

謝　辞

本研究の一部は平成 20・21・22 年度科学研究費補助金（特別研究員奨励費，課題番号：208222）の助成を受けた．

文　献

[1] Shepp LA, Vardi Y: Maximum likelihood reconstruction for emission tomography. IEEE Trans Med Imag **1**: 113-122, 1982

[2] Qi J, Leahy RM: Iterative reconstruction techniques in emission computed tomography. Phys Med Biol **51**: 541-578, 2006

[3] Hebert T, Leahy RM: A generalized EM algorithm for 3-D Bayesian reconstruction from Poisson data using Gibbs priors. IEEE Trans Med Imag **8**: 194-202, 1989

[4] Green PJ: Bayesian reconstruction from emission tomography data using a modified EM algorithm. IEEE Trans Med Imag **9**: 84-93, 1990

[5] Leahy RM, Yan X: Incorporation of anatomical MR data for improved functional imaging with PET. Lect Notes Comput Sci **511**: 105-120, 1991

[6] Gindi G, Lee M, Rangarajan A et al: Bayesian reconstruction of functional images using anatomical information as priors. IEEE Trans Med Imag **12**: 670-680, 1993

[7] Kulkarni K, Khurd P, Hsiao I et al: A channelized Hotelling observer study of lesion detection in SPECT MAP reconstruction using anatomical priors. Phys Med Biol **52**: 3601-3617, 2007

[8] 小林哲哉，工藤博幸：PET/SPECTにおける画像再構成と病変検出の統合．Med Imag Tech **26**: 233-239, 2008

[9] Kobayashi T, Kudo H: Fusion of image reconstruction and lesion detection using a Bayesian framework for PET/SPECT. 2008 IEEE Nuclear Science Symposium Conference Record: 3617-3624, 2008

[10] Mameuda Y, Kudo H: New anatomical-prior-based image reconstruction method for PET/SPECT. 2007 IEEE Nuclear Science Symposium Conference Record **6**: 4142-4148, 2007

[11] Segars WP: Development and application of the new dynamic NURBS-based cardiac-torso (NCAT) phantom, Ph.D. Dissertation, The University of North Carolina, 2001

[12] Barrett HH, Yao J, Rolland J et al: Model observers for assessment of image quality. Proc Natl Acad Sci **90**: 9758-9765, 1993

[13] Meyers KJ, Barrett HH: Addition of a channel mechanism to the ideal-observer model. J Opt Soc Am A **4**: 2447-2457, 1987

[14] Wollenweber SD, Tsui BM, Lalush DS et al: Comparison of Hotelling observer models and human observers in defect detection from myocardial SPECT imaging. IEEE Trans Nucl Sci **46**: 2098-2103, 1999

[15] Nuyts J, Bequé D, Dupont P et al: A concave prior penalizing relative differences for maximum-a-posteriori reconstruction in emission tomography. IEEE Tran Nucl Sci **49**: 56-60, 2000

Evaluation of Lesion Detection Capabilities of Anatomically Based MAP Image Reconstruction Methods Using the Computer Observer Model

Tetsuya KOBAYASHI[*1], **Hiroyuki KUDO**[*1]

[*1] *University of Tsukuba*

This study was conducted to evaluate the lesion detection capabilities of anatomically based maximum a posteriori (MAP) image reconstruction methods in emission computed tomography using the computer observer model. In lesion detection tasks, conventional anatomically based MAP reconstruction methods cannot preserve lesions not present in the anatomical image with high contrast and at the same time suppress noise in the background regions. We previously proposed a new anatomically based MAP reconstruction method called the SOS-MAP method, which is based on the spots-on-smooth image model in which the image is modeled by the sum of the smooth background image and the sparse spot image, and showed that the SOS-MAP method can overcome the above-mentioned drawback of conventional anatomically based MAP methods. However, the lesion detection capabilities of the SOS-MAP method remained to be clarified. In the present study, the computer observer model was used to evaluate the lesion detection capabilities of the SOS-MAP method, and it was found that the SOS-MAP method is superior to conventional anatomically based MAP methods for the detection of lesions.

Key words: Emission computed tomography, Image reconstruction, Anatomical information, Lesion detection, Computer observer

Med Imag Tech **28** (4): 214-222, 2010

小林哲哉（こばやし　てつや）

2006年千葉大・工・情画卒．2008年同大大学院・自然科学・修士課程了．現在，筑波大大学院・システム情報・博士後期課程在学中．日本学術振興会・特別研究員（DC1）．2007年・2008年に日本医用画像工学会大会奨励賞，2008年日本医用画像工学会論文賞を受賞．核医学診断装置のイメージングに関する研究に従事．日本核医学会，日本医学物理学会の各会員．

工藤博幸（くどう　ひろゆき）

1985年東北大・工・通信卒．1990年同大大学院博士課程了．現在，筑波大・システム情報・准教授．1990年電子情報通信学会論文賞，1991年・2001年・2006年日本医用画像工学会論文賞，2006年国際雑誌『Inverse Problems』High Lights受賞．工博．CTとPETを中心とした医用イメージング，画像処理の研究に従事．IEEE，電子情報通信学会の各会員．

COMMUNICATION www.rsc.org/molecularbiosystems | Molecular BioSystems

Imaging of cancer by redox-mediated mechanism: a radical diagnostic approach†

Zhivko Zhelev,[a] Rumiana Bakalova,*[a] Ichio Aoki,[a] Veselina Gadjeva[b] and Iwao Kanno[a]

Received 23rd July 2010, Accepted 23rd August 2010
DOI: 10.1039/c0mb00113a

The present study describes a new diagnostic approach for carcinogenesis based on the different tissue redox activity of normal and cancer-bearing mammalians and its visualization and estimation by cell permeable and DNA annealing probe (nitroxide-labeled nitrosourea) and magnetic resonance imaging.

In the July 2009 issue of *Nature Reviews Drug Discovery*, Trahootham *et al.* have summarized the advanced concepts about the role of reactive oxygen species (ROS) in carcinogenesis and cancer therapy.[1] Over 50 years experience in free radical biology and medicine shows that the normal cells of healthy mammalians are characterized with low steady-state level of ROS and some constant (referent) level of reducing equivalents (RE) (Fig. 1S, ESI†). Increasing ROS above the critical level provokes genomic instability and uncontrolled proliferation. The normal cells become malignant. The rapidly proliferative cancer cells require a lot of energy, which is accompanied by abnormal production and consumption of RE. On the other hand, the ROS in cancer cells have to be kept below the threshold level for induction of apoptosis and cell death, which is accompanied by antioxidant consumption. The substances necessary for energy production and proliferation, as well as the antioxidants in cancer are provided by the normal tissues of cancer-bearing mammalians. These "normal" tissues become deficient in antioxidants and RE, while the level of ROS in them is over the referent level characteristic for healthy mammalians. The conclusion is that the levels of ROS and RE are rather different in cancer and normal tissues and the abnormal generation of ROS provokes genomic instability and cancer development, which could be a key to the successful cancer therapy.

It is widely accepted that the balance between ROS and RE in cells and tissues determines their redox activity. Our study is directed to imaging of carcinogenesis by redox-mediated mechanism. We are assuming that the redox activities of normal (healthy) and cancer tissues are different and this parameter could be used as a diagnostic marker for carcinogenesis and a prognostic marker for the efficiency of cancer therapy.

Currently, there is no universal non-invasive methodology for estimation of ROS/RE balance and, respectively, for estimation of tissue redox activity in intact mammalians. In cells and tissues, the total ROS level is determined by the levels of superoxide radicals, hydrogen peroxide, nitric oxide radicals, end-products of lipid peroxidation, natural antioxidants, enzymatic antioxidant systems, *etc.* The total RE level is determined by the status of the endogenous redox pairs: NADH/NAD^+, NADPH/$NADP^+$, reduced/oxidized glutathione, reduced/oxidized ascorbic acid, *etc.* Each parameter is estimated separately.[1–6] The difference between ROS/RE balance of cancer and normal tissues are based on comparative analysis of one or several of these parameters and the conclusions are usually controversial.[1–6]

In the present study we propose a new approach for non-invasive imaging of tissue redox activity in intact healthy and cancer-bearing mammalians, which allows a differentiation of cancer development from normal (healthy) condition.

The method is based on redox cycle of nitroxide probes and their MRI contrast properties, which makes them useful molecular sensors for tissue redox activity (Fig. 1). The nitroxide radical (which is characterized by T_1 contrast properties) participates in electron-transfer reactions with ROS and RE with formation of non-contrast intermediate products (hydroxylamine and oxoammonium ion).[7–10] The rate constants of these reactions determine the MRI signal decay of nitroxide probe in living cells and tissues. In healthy mammalians, the half-life of MRI signal decay ($\tau_{1/2}$) in the selected region of interest (ROI; for example, brain tissue) could be considered as a reference steady-state level of tissue redox activity in norm. We supposed that in cancer-bearing mammalians, the half-life of MRI signal decay in the same or similar ROI has to be different from this reference level.

In our previous study we demonstrated that only *cell-permeable* nitroxide probes are appropriate for tissue redox imaging.[11,12] ROS and RE are predominantly produced and localized into the cells. Therefore, the probe is required to enter the cell to be able to interact with ROS and RE.

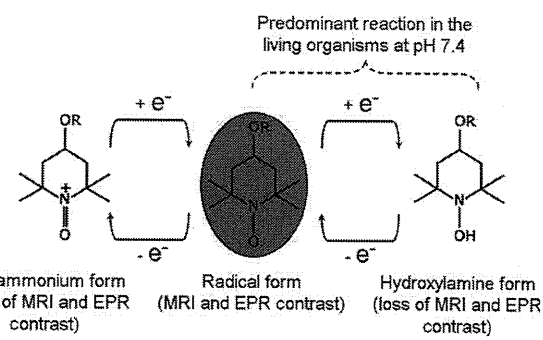

Fig. 1 Redox cycle of nitroxide radical and its MRI and EPR contrast properties.

[a] *Department of Biophysics, Molecular Imaging Center, NIRS, 4-9-1 Anagawa, Inage-ku, Chiba 263-8555, Japan. E-mail: bakalova@nirs.go.jp, ra_bakalova@yahoo.com; Fax: +81-43-206-3276; Tel: +81-43-206-4067*
[b] *Department of Chemistry and Biochemistry, Thrakia University, Stara Zagora, Bulgaria*

† Electronic supplementary information (ESI) available. Experimental details and supplementary figures. See DOI: 10.1039/c0mb00113a

In the present study, we used nitroxide-labeled nitrosourea (SLENU)—a cell-permeable and DNA annealing probe (Fig. 2S, ESI†). SLENU is a nitroxide-labeled analogue of the conventional anticancer drug CCNU (Lomustine).[13] LD50 (in mice) for SLENU was ~100 mg kg^{-1} b.w. *vs.* ~56 mg kg^{-1} b.w. for CCNU.[12] In the present study, SLENU was applied in 0.2–0.4 mmol kg^{-1} b.w. (single injection), which is below the LD50 value. In our previous studies, we established that the anticancer effect of SLENU is similar to that of CCNU.[12,13]

The animals (Balb6 nude mice) were separated in two groups: healthy mice (controls; $n = 6$) and mice with brain neuroblastoma (cancer-bearing mice; $n = 7$). In both groups, the mice were same age, almost same weight (~25 g), and kept under same conditions. Neuro2a cells (0.5×10^5 cells in 10 μL) were inoculated in one hemisphere of the brain and the MRI measurements were performed on the 7th–8th day after inoculation. Neuro2a cells initiate a development of brain neuroblastoma without significant angiogenesis within ~10 days after inoculation (Fig. 3S, ESI†). It allows us to ignore the MRI signal of nitroxide coming from the blood vessels, which is not indicative for tissue redox activity. Thus, the MRI signal of nitroxide probe in the tumor area could be considered as a result of its permeability and localization in the cancer cells.

The MRI measurements were performed on 7 tesla MRI. T_1-weighted incoherent gradient-echo sequence (fast low-angle shot; FLASH) was used (details are described in the ESI†). The animal was under anesthesia (1.5% isoflurane). The tail vein was canulated for drug administration. The MR imaging of mouse brain was started. After the 5th frame (scan-time ~1 min 40 s) during continuous scanning, the nitroxide was injected (100 μL per 25 g b.w.; single fast injection, within 15–20 s) and the MR imaging continued up to 40 frames (total scan-time ~14 min). Two ROI were selected: brain tissue (cortex) and soft tissues surrounding the brain (Fig. 3S, ESI†).

Fig. 2A shows a typical kinetics of MRI signal enhancement by SLENU in the brain of control mouse. The signal increased slightly after injection, followed by rapid decay. The first 5 frames (before injection of SLENU) were used for calculation of the averaged baseline level. All data were normalized to the baseline. The data were processed with *ImajeJ* software. The histograms in Fig. 2B represent the normalized data from 6 animals. The profiles of these histograms could be considered as reference profiles for the normal (healthy) condition of the respective tissue. In control mice, the half-life of MRI signal decay was about 1 min or 2 min 20 s in the brain or surrounding tissues, respectively. These $\tau_{1/2}$ values could be considered as reference values for the normal redox activity of the respective tissues. The profile of the histograms and $\tau_{1/2}$ values in Fig. 2 are indicative of a high reducing activity of the brain and surrounding tissues to the injected nitroxide radical.

In cancer-bearing mice, the profiles of time-dependent MRI signal enhancement by SLENU in the brain and surrounding tissues (Fig. 3) were completely different from that of the reference profiles, detected in control mice (Fig. 2B). The MRI signal intensity increased after the injection of nitroxide and remained high and stable over 14 min, without decay

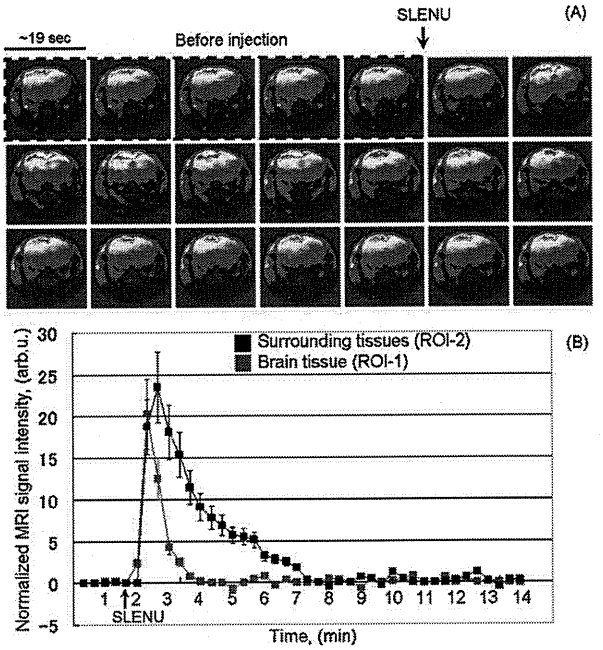

Fig. 2 (A) Time-dependent MR images (gradient-echo sequence) of the brain of normal (healthy) mouse before and after injection of SLENU. (B) MRI signal enhancement by SLENU in the brain (ROI-1) and surrounding tissues (ROI-2) under continuous scanning within 14 min. The data are mean ± SEM from 6 animals.

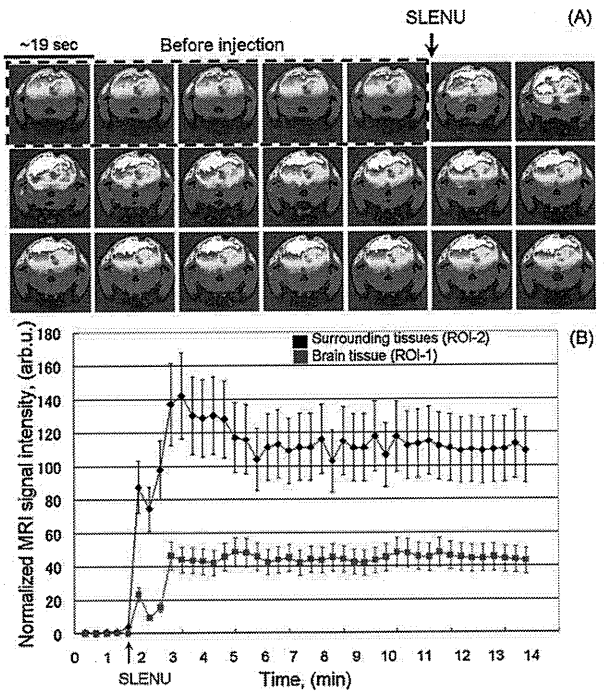

Fig. 3 (A) Time-dependent MR images (gradient-echo sequence) of the brain of cancer-bearing mouse before and after injection of SLENU. (B) MRI signal enhancement by SLENU in the brain (ROI-1) and surrounding tissues (ROI-2) under continuous scanning within 14 min. The data are mean ± SEM from 7 animals.

(Fig. 3A). In this case, the half-life of MRI signal decay can be considered over 14 min.

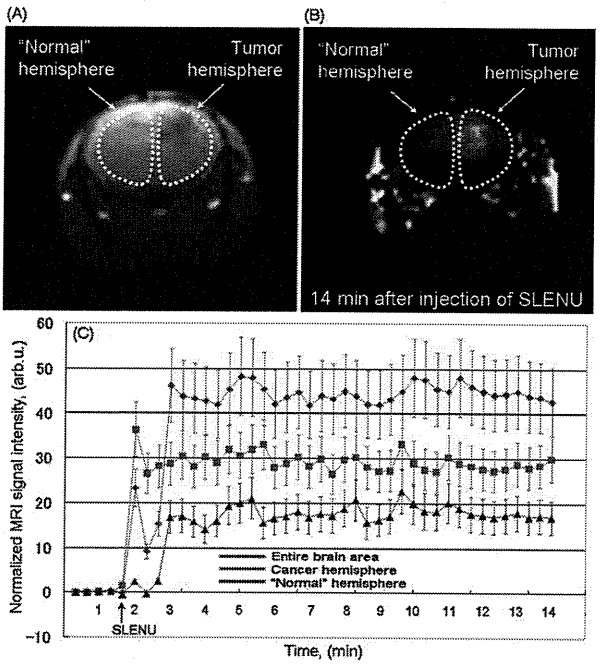

Fig. 4 (A) MR image (gradient-echo sequence) of tumor in mouse brain obtained 8 days after inoculation of cancer cells in Balb6 nude mouse. (B) Extracted MRI signal enhancement by SLENU, obtained 14 min after injection. The dotted lines indicate ROI—cancer hemisphere and "normal" hemisphere of the brain. (C) MRI signal enhancement by SLENU in the entire brain area, cancer hemisphere and "normal" hemisphere under continuous scanning within 14 min. The data are mean ± SEM from 4 animals.

In cancer-bearing mice, the profiles of the histograms were same in the cancer hemisphere of the brain, "normal" (non-cancer) hemisphere, and "normal" surrounding tissues (Fig. 4C). These profiles and $\tau_{1/2}$ values are indicative of a low reducing activity of the brain and surrounding "normal" tissues of cancer-bearing animals to the nitroxide probe. The "normal" tissues around the tumor have a different metabolic activity from the pre-cancer state, making them more sensitive to oxidation and damage.

Fig. 4b demonstrates the extracted MRI signal enhancement by SLENU from the original image, normalized to the baseline signal. It is well-seen that SLENU (as DNA annealing substance) is accumulated into the cancer tissue and the MRI signal is very high within 14 min after injection.

In a separate experiment *in vitro* using EPR spectroscopy, we investigated the amount of SLENU in extracted brain tissue after perfusion by saline solution. The brain was extracted ~5–10 min after injection of SLENU in the tail vein. The tissue homogenates were incubated with ferricyanide within 15 min. The ferricyanide quantitatively converts the reduced (non-EPR contrast) nitroxide to the oxidized (EPR contrast) radical form (Fig. 1). All tissue homogenates were treated at same conditions. Equal amounts of SLENU were detected in the brain of control mice and cancer-bearing mice—6.7 ± 1.2 pmol per mg tissue and 7.1 ± 0.9 pmol per mg tissue, respectively. Therefore, it can be concluded that the different MRI signal intensity and dynamics of SLENU in the brain of healthy and cancer-bearing mice is not a result of the different nitroxide concentration in the brain tissue. The different MRI signal dynamics of normal (healthy) and cancer tissues is a result of their different redox activity to the nitroxide radical.

In conclusion, the present study demonstrates a development of new diagnostic approach for carcinogenesis based on the different tissue redox activity of normal and cancer-bearing mammalians and its imaging by cell permeable nitroxide SLENU and MRI. There is a very clear difference between MRI signal enhancement by SLENU in healthy and cancer-bearing brain, which is indicative of the different metabolic activity of both tissues. In this case, the half-life of MRI signal decay is an appropriate diagnostic marker for carcinogenesis and a prognostic marker for the efficiency of cancer therapy. The described methodology is also applicable in isolated tissue specimens (*e.g.*, biopsy specimens).

This study also demonstrates that the piperidine-type nitroxide radical possesses a high contrast for MR imaging *in vivo* and this contrast is highly sensitive to the tissue redox activity.

Acknowledgements

The technical support of Ms Sayaka Shibata and Mr Shigeyoshi Saito (Molecular Imaging Center, NIRS-Chiba, Japan) are gratefully acknowledged. This study was partially supported by the JSPS through its "Funding Program for World-Leading Innovative R&D on Science and Technology" and Grand-in-aid "Kakenhi" No 21611011

References

1 D. Trachootham, J. Alexandre and P. Huang, *Nat. Rev. Drug Discovery*, 2009, **8**, 579.
2 J. Fang, T. Seki and H. Maeda, *Adv. Drug Delivery Rev.*, 2009, **61**, 290.
3 T. W. Miller, J. S. Isenberg and D. D. Roberts, *Chem. Rev.*, 2009, **109**, 3099.
4 J. R. Kanwar, R. K. Kanwar, H. Burrow and S. Baratchi, *Curr. Med. Chem.*, 2009, **16**, 2373.
5 G. Pani, E. Giannoni, T. Galeotti and P. Chiarugi, *Antioxid. Redox Signaling*, 2009, **11**, 2791.
6 M. Landriscina, F. Maddalena, G. Laudiero and F. Esposito, *Antioxid. Redox Signaling*, 2009, **11**, 2701.
7 G. M. Rosen, M. S. Cohen, B. E. Britigan and S. Pou, *Free Radical Res.*, 1990, **9**, 187.
8 B. P. Soule, F. Hyodo, K. Matsumoto, N. L. Simone, J. A. Cook, M. C. Krishna and J. B. Mitchell, *Antioxid. Redox Signaling*, 2007, **9**, 1731.
9 F. Hyodo, B. P. Soule, K. Matsumoto, S. Matsumoto, J. A. Cook, E. Hyodo, A. L. Sowers, M. C. Krishna and J. B. Mitchell, *J. Pharm. Pharmacol.*, 2008, **60**, 1049.
10 J. Trnka, F. H. Blaikie, R. A. Smith and M. P. Murphy, *Free Radical Biol. Med.*, 2008, **44**, 1406.
11 Z. Zhelev, R. Bakalova, I. Aoki, K. Matsumoto, V. Gadjeva, K. Anzai and I. Kanno, *Chem. Commun.*, 2009, (1), 53.
12 Z. Zhelev, R. Bakalova, I. Aoki, K. Matsumoto, V. Gadjeva, K. Anzai and I. Kanno, *Mol. Pharmaceutics*, 2009, **6**, 504.
13 V. Gadjeva, *Eur. J. Med. Chem.*, 2002, **37**, 295.

J Physiol Sci (2010) 60:399–406
DOI 10.1007/s12576-010-0108-9

ORIGINAL PAPER

Contribution of nitric oxide to cerebral blood flow regulation under hypoxia in rats

Hiroyuki Takuwa · Tetsuya Matsuura · Rumiana Bakalova · Takayuki Obata · Iwao Kanno

Received: 21 March 2010 / Accepted: 2 August 2010 / Published online: 7 October 2010

Abstract This study was designed to clarify whether nitric oxide (NO) participates in the regulation of local cerebral blood flow (CBF) during hypoxia (inhalation of 15% O_2 in N_2). The CBF response to hind-paw stimulation (evoked CBF) of Sprague-Dawley (SD) rats was measured by laser-Doppler flowmetry. Physiological variables, such as heart rate, mean blood pressure, and $PaCO_2$ during hypoxia, were identical to those under normoxic conditions. Hypoxia increased the baseline CBF (17.5 ± 14.3%) and the normalized peak amplitude of evoked CBF (31.1 ± 18.5%) relative to those during normoxia. When an NOS inhibitor was infused intravenously, these differences were abolished in both the baseline CBF or evoked CBF between normoxic and hypoxic conditions, whereas the heart rate decreased and the mean blood pressure increased during hypoxia in comparison with these during normoxia. The field potential was constant under all experimental conditions. These results suggest that NO plays a major role in the regulation of baseline and evoked CBF during hypoxia.

Keywords Cerebral blood flow · Functional activation · Laser-Doppler flowmetry · Somatosensory stimulation · Rat · Nitric oxide

H. Takuwa (✉) · T. Matsuura · R. Bakalova · T. Obata · I. Kanno
Department of Biophysics, Molecular Imaging Center, National Institute of Radiological Sciences, 4-9-1 Anagawa, Chiba 263-8555, Japan
e-mail: takuwa@nirs.go.jp

T. Matsuura (✉)
Academic Group of Mathematical and Natural Science, Iwate University, 4-3-5 Ueda, Morioka 020-8551, Japan
e-mail: matsuura@iwate-u.ac.jp

Introduction

Changes in local cerebral blood flow (CBF) are closely related to neural activity; therefore, the cerebral hemodynamic response has been used extensively to map brain function in humans and animals. One of the major roles of CBF is to supply oxygen to the brain tissues. The relationship between oxygen metabolism and CBF is of considerable interest to many researchers.

In the case of baseline CBF, it has been reported that an increased arterial oxygen supply (hyperoxia) results in a decrease in the baseline level of CBF in rats [1], whereas a decreased arterial oxygen supply (hypoxia) increases the baseline level of CBF in humans [2] and in the somatosensory cortex of rats [3–5]. These observations indicate that the baseline CBF is affected by the O_2 level in the supplying blood in brain tissue.

On the other hand, in the case of an increase in local CBF (evoked CBF), induced by neuronal activation, the relationship between evoked CBF and blood oxygenation in the activated brain area is still a disputable and controversial issue. In our previous study, we reported that hyperoxia provokes the enhancement of evoked CBF in the V1 area of the human brain [6, 7] and in the somatosensory cortex of rats [1]. In a human study, using positron emission tomography (PET), Mintun et al. [2] reported that hypoxia does not enhance evoked CBF, suggesting that evoked CBF is independent of the oxygen supply or metabolic demand. In contrast, several studies in rats, using functional magnetic resonance imaging (fMRI) and optical spectroscopy, showed that hyperoxia provokes a decrease in evoked CBF, while hypoxia induces its enhancement [3, 4, 8]. These studies suggest that evoked CBF depends on the oxygen metabolic demand.

The dynamics of the evoked CBF is highly complicated and many biochemical mediators could be considered in

the regulation system, such as nitric oxide (NO), cyclo-oxygenase-1 (COX-1), COX-2, and adenosine [9–11]. NO, produced by endothelial and neuronal nitric oxide synthase (NOS), acts as a neurotransmitter and is involved in the regulation of cerebral circulation. In particular, it is also an important mediator of the cerebral vasodilatation in response to changes in the physiological parameters during hypercapnia [12] and hyperoxia [1]; however, the role of NO in evoked CBF regulation remains to be elucidated. In our previous study, we reported that the NOS inhibition was accompanied by a decrease in baseline CBF during normoxia and suppression of evoked CBF during hyperoxia [1]. We speculated that NOS inhibition would also suppress the effect of hypoxia on cerebral circulation.

In the present study, we investigated the effect of hypoxia on the baseline levels of CBF and evoked CBF using laser-Doppler flowmetry (LDF) to clarify the regulation mechanism of CBF in relation to the metabolic oxygen demand. The effect of NOS inhibition on CBF regulation under hypoxia was also demonstrated using N^{ω}-nitro-L-arginine (LNA) as a pharmacological tool.

Materials and methods

Animal preparation and control of physiological conditions

All experiments were conducted in accordance with the guidelines of the Physiological Society of Japan and were approved by the Animal Care and Use Committee of the National Institute of Radiological Sciences, Chiba, Japan.

Sprague-Dawley rats (370–420 g) were anesthetized with isoflurane (4% for induction and 1.5% during surgery) in 30% O_2 and 70% N_2 using a face mask. Subcutaneous 2% lidocaine was used before incision to prevent vasospasm during catheter insertion. The tail artery and left femoral vein were cannulated for blood pressure monitoring, blood gas sampling, and intravenous drug administration. After tracheotomy, α-chloralose (75 mg/kg body weight, i.v.) was administered and isoflurane administration was discontinued. Anesthesia was maintained with α-chloralose (44 mg/kg/h, i.v.), and muscle relaxation was maintained with pancuronium bromide (0.7 mg/kg/h, i.v.) during the experimental period. Body temperature was monitored with a rectal probe and maintained at approximately 37.0°C using a heating pad (ATC-210; Unique Medical, Japan). The rat was fixed in a stereotactic frame, and the parietal bone was thinned to translucency at the left somatosensory cortex using a dental drill (an area 3 × 3 mm, centered 2.5 mm caudal and 2.5 mm lateral to the bregma). To ensure a stable physiological condition of the animal, the measurements were performed 3 h after the preparation of the parietal bone (Fig. 1).

The rat was paralyzed by injection of pancuronium bromide and artificially ventilated using a respirator (SN-480-7; Shinano, Japan) with a mixture of N_2 and O_2 to achieve physiological arterial blood levels of O_2 and CO_2 tension (PaO_2 and $PaCO_2$, respectively). During the experiments, the changes in respiratory O_2 and CO_2 concentrations were monitored with a capnometer (SurgiVet V9004, Smiths Medical, USA). Arterial blood pressure

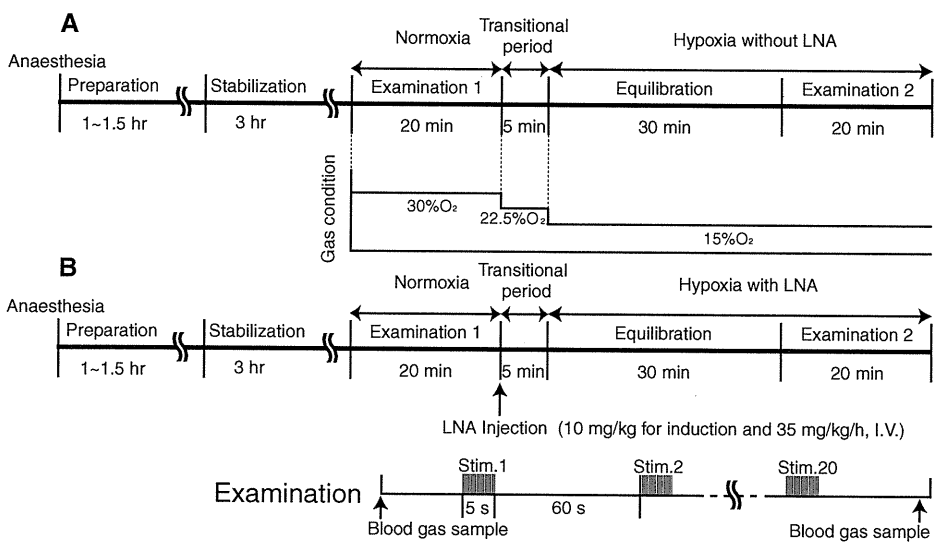

Fig. 1 Experimental protocol of hypoxia **a** without LNA (experiment A) and **b** hypoxia with LNA (experiment B). The experiment was carried out approximately 3 h after the preparation of rats. The evoked CBF and field potential were measured under normoxia, hypoxia without LNA, and hypoxia with LNA. In each examination, 20 successive stimuli (5 Hz and 5 s) were applied at 60 s intervals. The animals were ventilated with a 30% O_2 and 70% N_2 mixture during normoxia (control). To avoid a change in arterial blood pressure, the O_2 concentration was gradually decreased in a stepwise manner from 30 to 22.5 and 15% during hypoxia

Table 1 Physiological variables

Condition	Heart rate (b.p.m.)	MABP (mmHg)	$PaCO_2$ (mmHg)	PaO_2 (mmHg)
(A) Protocol A ($n = 9$)[a]				
Normoxia	379.4 ± 40.6	88.8 ± 7.7	36.9 ± 2.3	93.3 ± 11.0 ┐
Hypoxia without LNA	403.4 ± 35.0	92.3 ± 8.2	34.9 ± 1.9	49.8 ± 3.0 ┘*
(B) Protocol B ($n = 8$)[a]				
Normoxia	360.3 ± 19.7 ┐	98.0 ± 11.0 ┐	35.9 ± 2.3	101.8 ± 11.9 ┐
Hypoxia with LNA	315.3 ± 30.3 ┘*	134.6 ± 4.6 ┘*	36.9 ± 1.2	48.1 ± 1.4 ┘*

[a] Number of rats; mean ± SD

* $P < 0.01$

from the tail artery was measured with a pressure sensor (TP400T; Nihon Kohden, Japan) and recorded continuously using MacLab data acquisition software (AD Instruments, Australia) during the experiments; the mean arterial blood pressure (MABP) was calculated as the average at three time points (i.e., before, during, and immediately after each stimulation period). Arterial blood samples were serially collected before and immediately after each step of the experiment and analyzed for gas values.

Baseline and evoked CBF measurements

The evoked CBF was measured by LDF (FLO-C1; OMEGA FLO) equipped with a probe with a tip diameter of 0.55 mm (Probe NS; OMEGA FLO). The sampling volume for the LDF measurement was approximately 1 mm^3 [13]. A time constant of 0.1 s was used to detect the LDF signal. The LDF probe was positioned over the thinned skull (over the somatosensory area of the hind paw). Electrical hind paw stimulation was performed with two needle electrodes inserted subdermally into the right hind paw contralateral to the LDF probe. A current stimulus of 1.5 mA (0.1 ms pulse) was applied at 5 Hz frequency and 5 s duration. In each experiment, 20 successive stimuli were applied at 60 s intervals and accumulated using MacLab data acquisition software. These stimulus parameters did not cause any change in the systemic arterial blood pressure and heart rate during stimulation.

The evoked CBF response to somatosensory stimulation was investigated under three experimental conditions as follows: normoxia (17 rats), hypoxia without LNA (9 rats), and hypoxia with LNA (8 rats) (Fig. 1).

Hypoxia and application of NOS inhibitor

Under normoxia (control), the animals were ventilated with a 30% O_2 and 70% N_2 mixture. Hypoxia was induced by decreasing the concentration of inspired O_2 to 15%. The acute change from 30% O_2 to 15% O_2 often caused mild hypotension, so the O_2 concentration was gradually decreased in a stepwise manner from 30 to 22.5% and 15% (Fig. 1). This stepwise hypoxia had no effect on arterial blood pressure (Table 1). In the "hypoxia without LNA" experiment (Fig. 1a), we first examined the evoked CBF under normoxia. The oxygen concentration was then decreased in a stepwise manner from 30 to 22.5% and 15%. After an equilibration time of 30 min, the evoked CBF was measured during hypoxia without LNA. In the "hypoxia with LNA" experiment (Fig. 1b), we also examined the evoked CBF under normoxia. LNA was then applied intravenously (10 mg kg^{-1} for induction and 35 mg kg^{-1} h^{-1} during experiments), and the O_2 concentration was decreased in a stepwise manner from 30 to 22.5% and 15%. After an equilibration time of 30 min, evoked CBF responses were measured under hypoxia with LNA administration.

Measurement of neuronal activity

To estimate the correlation between the change in evoked CBF and neuronal activation, field potentials were measured in both experiments: "hypoxia without LNA" (6 rats) and "hypoxia with LNA" (6 rats). A tungsten microelectrode (12 MΩ) was inserted into the somatosensory area of the hind paw through the thinned portion of the skull and fixed using dental cement. The tip of the electrode was set at a depth of approximately 0.5 mm from the surface of the cortex. An Ag-AgCl indifferent electrode was placed between the skull bone and scalp. Field potentials under normoxia, hypoxia without LNA, and hypoxia with LNA were recorded using the same time schedule as evoked CBF measurements (Fig. 1). Twenty successive signals of the field potential recordings were also accumulated using MacLab data acquisition software and were digitized at 100 Hz, which was the same frequency as that in our previous study [1, 11, 14]. The mean amplitude of the field potentials was calculated as the average of the negative components of each spike to evaluate the neuronal activity during stimulation [1, 14].

Data analysis

The LDF signal was normalized towards the baseline level as percent changes from the baseline (normalized evoked

CBF). The rise time of the evoked CBF was defined as the time at the intersection of the extrapolated lines, which was drawn with the baseline on the response curve from 90 to 10% of the peak [15, 16]. The peak amplitude indicated the percent change from the baseline to the maximum evoked CBF. Values were statistically analyzed by Student's *t* test and presented as the mean ± SD.

Results

Physiological variables during hypoxia and LNA administration

The physiological variables (i.e., heart rate, MABP, and $PaCO_2$) during hypoxia without LNA were almost identical to those during normoxia (control) (Table 1). Only the PaO_2 value (49.8 ± 3.0 mmHg) was significantly different from that measured during normoxia (PaO_2 = 93.3 ± 11.0 mmHg) ($P < 0.01$).

The systemic administration of the NOS inhibitor LNA during hypoxia (hypoxia with LNA) significantly increased MABP and decreased the heart rate relative to those parameters during normoxia ($P < 0.01$). PaO_2 was significantly lower during hypoxia with LNA (48.1 ± 1.4 mmHg) than during normoxia (101.8 ± 11.9 mmHg) ($P < 0.01$). There was no clear change in the respiratory CO_2 concentration between normoxia and hypoxia (data not shown).

Effects of hypoxia on CBF

During hypoxia (in the absence of LNA), the baseline level of CBF was significantly higher than that during normoxia ($P < 0.05$) (Fig. 2). As shown in Fig. 3a, hypoxia enhanced the normalized evoked CBF in comparison with normoxia. There was a significant difference in the peak amplitude of the normalized evoked CBF between the hypoxic condition (20.4 ± 7.4%) and normoxic condition (15.3 ± 5.4%) ($P < 0.05$) (Fig. 3b). The rise time of evoked CBF was 0.67 ± 0.22 s during hypoxia and 0.51 ± 0.30 s during normoxia, although no significant difference in the rise time between the two conditions was detected. Presumably, some mediators involved in vasodilatation enhance baseline and evoked CBF during hypoxia. In the subsequent experiments, we focused on NO as one of the possible candidates responsible for vasodilatation.

Application of NOS inhibitor during hypoxia

The injection of NOS inhibitors (LNA) in rats subjected to hypoxia resulted in the same baseline CBF as that during normoxia (Fig. 2). The normalized evoked CBF during

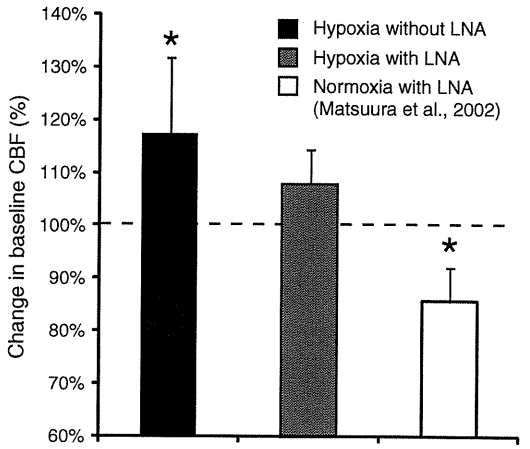

Fig. 2 Change in baseline CBF. The values of baseline CBF, obtained during normoxia, were considered to be 100%, indicated by *a dashed line*. *Black* and *gray bars* indicate the baseline CBF during hypoxia without LNA and hypoxia with LNA, respectively. The *white bar* indicates the baseline CBF during normoxia with LNA, which was obtained in the previous study [1]. The data were normalized to those under normoxia without LNA after statistical analysis. To evaluate the changes in baseline CBF, the absolute value of the baseline CBF was statistically compared for each animal group by paired *t* test. Note that the baseline CBF during hypoxia with LNA was not significantly different from that during normoxia, whereas the baseline CBF was higher during hypoxia without LNA than during normoxia. *Asterisks* indicate significant differences in levels of baseline CBF between hypoxia without LNA and normoxia without LNA, and normoxia with LNA and normoxia without LNA ($P < 0.05$). *Error bars* are SD

hypoxia with LNA did not increase in comparison with that during normoxia (Fig. 4b). The peak amplitude of the normalized evoked CBF was 22.8 ± 10.8% during normoxia and 19.5 ± 7.6% during hypoxia with LNA (Fig. 4c). A slight (but not significant) decrease in the evoked CBF was detected in rats subjected to hypoxia and with LNA. There was no significant difference in the rise time of evoked CBF between normoxia and hypoxia with LNA: 0.60 ± 0.23 s during hypoxia with LNA and 0.57 ± 0.29 s during normoxia. The results suggest that NO is involved in the enhancement of baseline and evoked CBF during hypoxia. The NO inhibitor abolished the effect of hypoxia completely at the baseline level and evoked CBF; therefore, NO could be considered as a major mediator of the relationship between hypoxia and evoked CBF response.

Neural activities during experiments

Figure 5 shows one of the representative field potentials from the somatosensory cortex during normoxia, hypoxia without LNA, and hypoxia with LNA. The field potential during hypoxia without LNA was almost the same as that during normoxia (Fig. 5a). There were no significant differences in the mean amplitude and number of spikes of

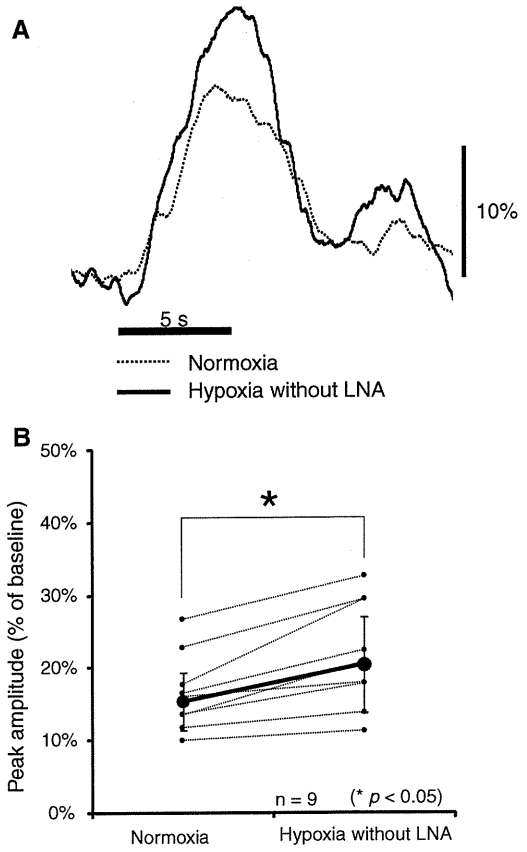

Fig. 3 Change in normalized evoked CBF under normoxia and hypoxia without LNA. **a** Normalized evoked CBF with somatosensory stimulation from one representative animal. Curves were normalized to the baseline level. *Horizontal* and *vertical bars* indicate the stimulation period and 10% increase from the baseline level, respectively. **b** Peak amplitude of normalized evoked CBF under normoxia and hypoxia without LNA. *Each line* corresponds to the data obtained from one rat. *Bold lines* and *error bars* indicate the mean value and SD, respectively ($n = 9$). Note that the normalized evoked CBF was significantly higher during hypoxia than during normoxia ($^*P < 0.05$)

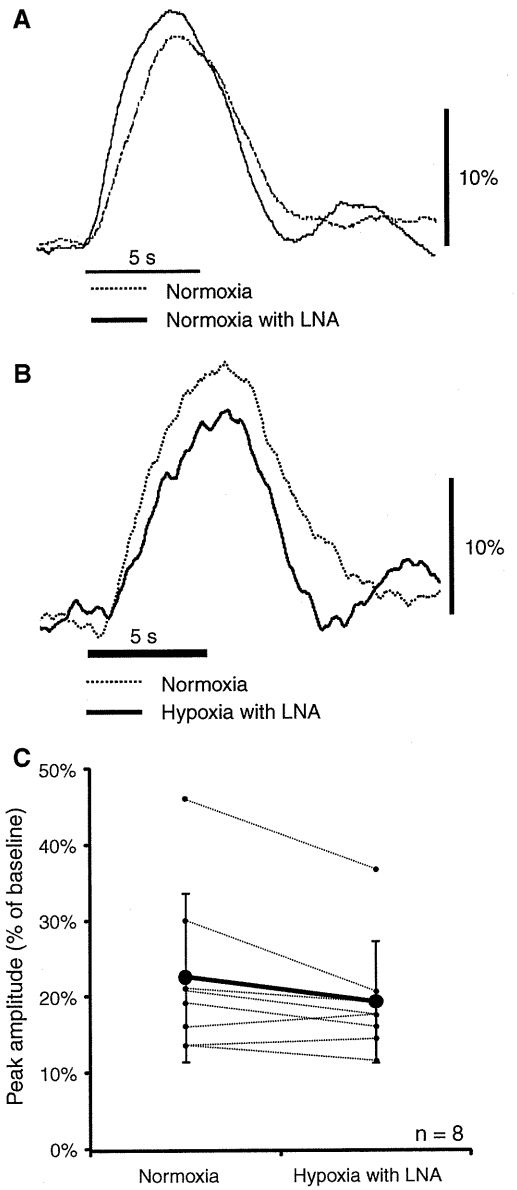

Fig. 4 Change in normalized evoked CBF during normoxia, normoxia with LNA, and hypoxia with LNA. **a** Normalized evoked CBF during normoxia without LNA and normoxia with LNA (cited from reference [1]). **b** Normalized evoked CBF during normoxia without LNA and hypoxia with LNA. Curves were normalized to the baseline level and shown for one representative animal. *Horizontal* and *vertical bars* indicate the stimulation period and 10% increase from baseline level, respectively. **c** Peak amplitude of normalized evoked CBF under normoxia and hypoxia with LNA. Each *line* corresponds to the data obtained from one rat. *Bold lines* and *error bars* indicate the mean value and SD, respectively ($n = 8$). No significant difference in the peak amplitude of normalized evoked CBF between normoxia and hypoxia with LNA was observed

field potentials between hypoxia without LNA and normoxia (Table 2). The results indicate that the enhancement of evoked CBF is not caused by an increase in neuronal activity during hind paw stimulation.

The field potential during hypoxia with LNA was also almost the same as that during normoxia (Fig. 5b). There were no significant differences in the mean amplitude and number of spikes of field potentials between hypoxia with LNA and normoxia (Table 2), indicating that the application of LNA did not affect neuronal activity.

Discussion

In the present study, we investigated the effects of hypoxia on the regulation of baseline and evoked CBF in rats, as well as the role of NO in this relationship. NO is synthesized mainly by endothelial NOS (eNOS), neuronal NOS (nNOS), and inducible NOS (iNOS) in the brain tissue. To

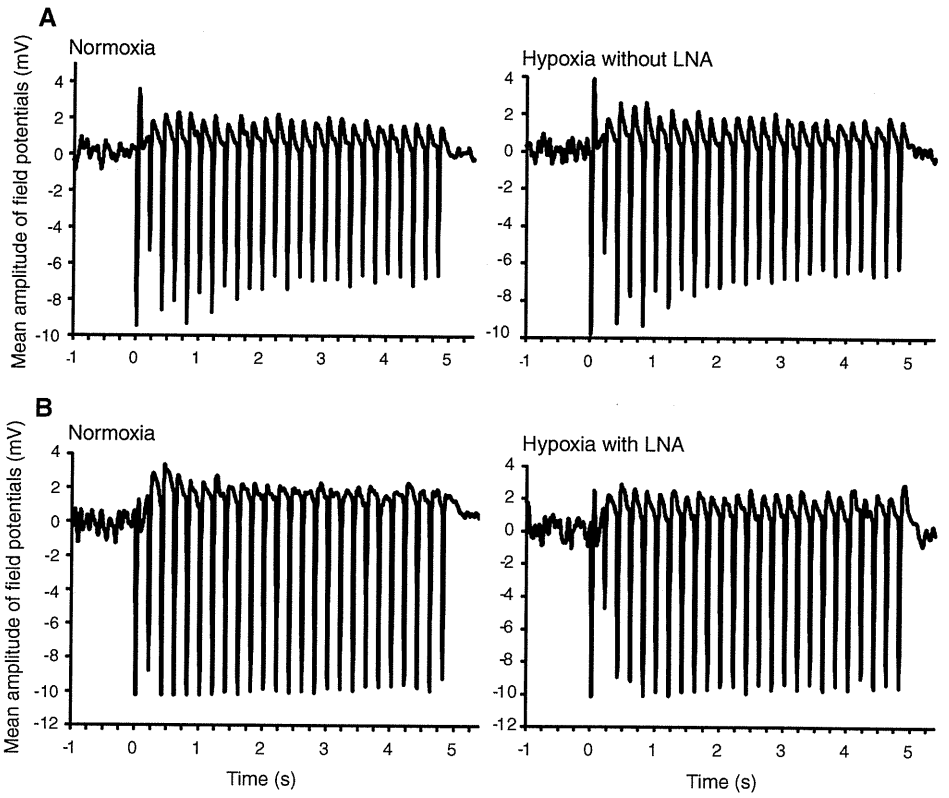

Fig. 5 Representative field potential recordings from the somatosensory cortex during hind paw stimulation. **a** Hypoxia without LNA. Neuronal activity during hypoxia without LNA was almost the same as that during normoxia. **b** Hypoxia with LNA. Field potential during hypoxia with LNA was almost identical to that during normoxia. In both experiments, there were no significant differences in the mean amplitude and number of spikes of field potentials between hypoxia and normoxia (see Table 2)

Table 2 Parameters of neuronal activity during each examination

Condition	Mean amplitude of field potentials (mV)	Number of spikes detected
(A) Protocol A ($n = 6$)[a]		
Normoxia	−4.3 ± 3.3] NS	20.8 ± 6.1] NS
Hypoxia without LNA	−4.3 ± 3.5]	20.8 ± 6.1]
(B) Protocol B ($n = 6$)[a]		
Normoxia	−6.3 ± 2.3] NS	17.2 ± 5.8] NS
Hypoxia with LNA	−6.4 ± 2.3]	17.2 ± 5.7]

Hind-paw stimulation (5 Hz and 5 s)

NS not significant

[a] Number of rats; mean ± SD

inhibit the activities of all these NOS isoenzymes, a non-selective NOS inhibitor, LNA, was used. A previous study showed that the intracortical administration of the NOS inhibitor affected the CBF during hypoxia [17]. We also found that the NOS inhibitor LNA infused intravenously attenuated the CBF response to hyperoxic conditions [1]. The intravenous infusion of LNA may cause excess accumulations of the drug leading to unfavorable effects on the evoked CBF. However, we revealed that the systemic administration of LNA under normoxic condition (normoxia with LNA) did not affect the neuronal activity and normalized evoked CBF (Fig. 4a), although it caused a decline in the level of the baseline CBF (Fig. 2) [1]. The experimental protocol used in this study should not cause any side effects of the drug leading to the normalized evoked CBF.

It has been reported that hypoxia causes mild hypotension [4, 5]. In our experiment, we avoided a significant reduction of MABP during hypoxia by applying a stepwise decrease in the inspired O_2 concentration and mild hypoxia (15% O_2) (Fig. 1). The other physiological parameters (i.e., heart rate and $PaCO_2$) during hypoxia were identical to those during normoxia (Table 1), which is in agreement with the previous report [5]. It is known that hypoxia activates distinct cellular and molecular processes in the brain depending on both its severity and time course (e.g., rate of decrease in oxygen tension and duration). The protocol in the hypoxia experiment was targeting PaO_2 within 40–50 mmHg, which was consistent with previous studies [3–5], but kept the $PaCO_2$, MABP, and heart rate within the normal range. The stepwise method of hypoxia used in this study is one of the best ways to achieve this and did not cause any serious damage to the brain tissue. Moreover, the inhalation of 15% O_2 in N_2 did not evoke a hypoxic ventilatory response (i.e., increases in minute ventilation) despite the fact that PaO_2 was significantly lowered (Table 1). In this study, rats were anesthetized and relaxed with continuous infusion of α-chloralose and pancuronium bromide during the experiment. Muscle relaxation with pancuronium bromide does not cause hypoxic ventilatory responses.

We reported that the baseline CBF was ~5.0% lower during hyperoxia than during normoxia [1], and we found in the present study that it was ~17.5% higher during hypoxia than during normoxia (Fig. 2). These results indicate that the baseline CBF under resting conditions is regulated to maintain a constant oxygen supply. The infusion of LNA in rats during hypoxia abolished the effect of hypoxia and returned the baseline to the level obtained during normoxia (Fig. 2). A decrease in the baseline CBF under normoxia with LNA has been reported (Fig. 2) [1]. Their results suggest that the systemic administration of LNA suppresses the NO activity and the decline in the baseline CBF. We considered that the increase in the baseline CBF during hypoxia was caused by an increase in the level of NO activity.

Mintun et al. [2] reported following a PET study that there is no significant difference in the normalized regional CBF response to visual stimulation between normoxia and hypoxia and that the baseline level of CBF is higher during hypoxia than during normoxia. The discrepancy between our findings and the results of the PET study might be a result of the differences in experimental protocols and measurement techniques. For example, the time resolution of LDF in this study is much higher than that of PET. A higher time resolution of LDF is feasible in detecting the detailed time course of evoked CBF during hypoxia. Thus, it is possible that an increase in evoked CBF during hypoxia could be detected in our present LDF study that might have been smoothed out in the PET study.

The peak amplitude of normalized evoked CBF is higher under hyperoxia than under normoxia [1, 7]. The normalized evoked CBF during hypoxia was also enhanced in comparison with that during normoxia (Fig. 3). These observations suggest that the evoked CBF is enhanced by abnormal oxygen supply, such as high and low levels of oxygen in the brain tissue. The peak amplitude of normalized evoked CBF during hypoxia with LNA was also the same as that during normoxia (Fig. 4b). We previously reported that LNA administration during hyperoxia decreased not only evoked CBF but also the neural activity. Therefore, the increase in the evoked CBF during hyperoxia was not simply accounted for by the up-regulated NOS expression. On the other hand, there was no significant difference in neuronal activity between normoxia and hypoxia with LNA (Fig. 5; Table 2). These observations suggest that hypoxia is accompanied by an increase in NOS activity, and that LNA administration during hypoxia suppresses this process.

It has been reported that although the baseline CBF is higher during hypercapnia than that during normocapnia, there was no significant difference in normalized evoked CBF between the hypercapnic and normocapnic conditions [18]. These results indicated that the absolute value of evoked CBF increases according to the baseline CBF during hypercapnia; that is, the evoked CBF under hypercapnia is proportional to the baseline CBF. In contrast, we established that the normalized evoked CBF is higher during hypoxia than during normoxia despite the increase in baseline CBF (Fig. 3). This suggests that there are some differences in the mechanism of NOS activity between hypercapnia and hypoxia. Since hypoxia is accompanied by free radical generation in the hypoxic area [19], it may be speculated that nitric oxide radicals and their intermediate products are involved in the regulation of evoked CBF response during hypoxia, while hypercapnia is not accompanied by such free radical mechanism.

A previous study showed that the increase in neuronal activity induced by stimulation in rat was unchanged during acute hypoxia relative to that under normoxia [3]. As mentioned above, in the present study, hypoxia was caused by a stepwise mild decrease in the respiratory O_2 concentration. The neuronal activity was not significantly different between hypoxia and normoxia (Fig. 5; Table 2), suggesting that the neural activity induced by stimulation is stable during the experiment. The enhancement of evoked CBF during hypoxia in this study may be caused by a low oxygen supply level within the activated brain area.

It is well known that NO is a key mediator of cerebrovascular responses to carbon dioxide and involved in neurovascular coupling. However, the effects of NOS inhibitors, such as LNA, on the neurovascular coupling differ with each experimental condition. LNA by itself reduced the evoked CBF slightly but not completely. This is because the CBF response to neuronal activation is mediated by various mediators, e.g., NO, prostaglandins, adenosine, and ions [11, 16]. LNA blocks only NO synthesis, but not the effects of other mediators of neurovascular coupling. In our study, we observed that LNA abolished completely the effect of hypoxia on the evoked CBF response. Moreover, the evoked CBF response is slightly lower in the presence of LNA than under normoxia (Fig. 4). This means that a part of the evoked CBF response to normoxia, but not the total response, could be explained by the effect of NO.

Acknowledgments The present work was supported by a grant from the Ministry of Education, Culture, Sports, Science and Technology of Japan, and KAKENHI from the Japan Society for the Promotion of Science.

References

1. Matsuura T, Kanno I (2002) Effect of nitric oxide synthase inhibitor on the local cerebral blood flow evoked by rat somatosensory stimulation under hyperoxia. Comp Biochem Physiol A 131:267–274

2. Mintun MA, Lundstrom BN, Snyder AZ, Vlassenko AG, Shulman GL, Raichle ME (2001) Blood flow and oxygen delivery to human brain during functional activity: theoretical modeling and experimental data. Proc Natl Acad Sci USA 98:6859–6864
3. Lindauer U, Gethmann J, Kühl M, Kohl-Bareis M, Dirnagl U (2003) Neuronal activity-induced changes of local cerebral microvascular blood oxygenation in the rat: effect of systemic hyperoxia or hypoxia. Brain Res 975:135–140
4. Sicard KM, Duong TQ (2005) Effects of hypoxia, hyperoxia, and hypercapnia on baseline and stimulus-evoked BOLD, CBF, and CMRO2 in spontaneously breathing animals. Neuroimage 25:850–858
5. Sukhotinsky I, Dilekoz E, Moskowitz MA, Ayata C (2008) Hypoxia and hypotension transform the blood flow response to cortical spreading depression from hyperemia into hypoperfusion in the rat. J Cereb Blood Flow Metab 28:1369–1376
6. Kanno I, Fujita H, Hatazawa J (1996) Enhancement of CBF response for V1 stimuli during hyperoxia: behavior of oxygen in neuronal activation revisited. J Cereb Blood Flow Metab 17:S646
7. Kashikura K, Kershaw J, Kashikura A, Matsuura T, Kanno I (2000) Hyperoxia-enhanced activation-induced hemodynamic response in human VI: an fMRI study. Neuroreport 11:903–906
8. Duong TQ (2007) Cerebral blood flow and BOLD fMRI responses to hypoxia in awake and anesthetized rats. Brain Res 1135:186–194
9. Magistretti PJ, Pellerin L, Rothman DL, Shulman RG (1999) Energy demand. Science 22:496–497
10. Iadecola C (2004) Neurovascular regulation in the normal brain and in Alzheimer's disease. Nat Rev Neurosci 5:347–360
11. Matsuura T, Takuwa H, Bakalova R, Obata T, Kanno I (2009) Effect of cyclooxygenase-2 on the regulation of cerebral blood flow during neuronal activation in the rat. Neurosci Res 65:64–70
12. Iadecola C (1992) Does nitric oxide mediate the increases in cerebral blood flow elicited by hypercapnia? Proc Natl Acad Sci USA 89:3913–3916
13. Solfrizzi V, D'Introno A, Colacicco AM, Capurso C, Del Parigi A, Capurso S, Gadaleta A, Capurso A, Panza F (2005) Dietary fatty acids intake: possible role in cognitive decline and dementia. Exp Gerontol 40:257–270
14. Matsuura T, Kanno I (2001) Quantitative and temporal relationship between local cerebral blood flow and neuronal activation induced by somatosensory stimulation in rats. Neurosci Res 40:281–290
15. Matsuura T, Fujita H, Seki C, Kashikura K, Kanno I (1999) CBF change by somatosensory activation measured by laser-Doppler flowmetry: independent evaluation of RBC velocity and RBC concentration. Jpn J Physiol 49:289–296
16. Bakalova R, Matsuura T, Kanno I (2002) The cyclooxygenase inhibitors indomethacin and rofecoxib reduce regional cerebral blood flow evoked by somatosensory stimulation in rats. Exp Biol Med (Maywood) 227:465–473
17. Pelligrino DA, Wang Q, Koenig HM, Albrecht RF (1995) Role of nitric oxide, adenosine, *N*-methyl-D-aspartate receptors, neuronal activation in hypoxia-induced pial arteriolar dilation in rats. Brain Res 704:61–70
18. Matsuura T, Fujita H, Kashikura K, Kanno I (2000) Evoked local cerebral blood flow induced by somatosensory stimulation is proportional to the baseline flow. Neurosci Res 38:341–348
19. Packer L, Prillipko L, Christen Y (eds) (1992) Free radicals in the brain. Springer, Berlin